Acquiring, Analyzing, and Using Complete Three-Dimensional Aggregate Shape Information

by

E. J. Garboczi and N.S. Martys
Building and Fire Research Laboratory
National Institute of Standards and Technology
Gaithersburg, MD 20899 USA

and

Habeeb H. Saleh and Richard A. Livingston
Turner Fairbank Highway Research Center
Federal Highway Administration
6300 Georgetown Pike
McLean, VA 22101

Reprinted from AGGREGATES, Concrete, Bases, and Fines, 9th Annual Symposium, Proceedings (CD-ROM). Center for Aggregates Research. April 22-25, 2001, Austin, Texas, 13 pp, 2001.

NIST
National Institute of Standards and Technology
Technology Administration, U.S. Department of Commerce

ACQUIRING, ANALYZING, AND USING COMPLETE THREE-DIMENSIONAL AGGREGATE SHAPE INFORMATION

E.J. GARBOCZI and N.S. MARTYS
National Institute of Standards and Technology
100 Bureau Drive Stop 8621
Gaithersburg, MD 20899-8621

HABEEB H. SALEH and RICHARD A. LIVINGSTON
Turner Fairbank Highway Research Center,
Federal Highway Administration
6300 Georgetown Pike
McLean, VA 22101

Abstract

The shape of aggregates, from whatever source, plays a crucial role in determining the properties of the composite material in which they are embedded (e.g., asphaltic or portland cement concrete). To properly characterize this three-dimensional shape, three-dimensional information is needed. We show how this kind of information can be acquired via x-ray computed tomography. Mathematical "burning" algorithms can be applied to a multi-aggregate image to extract individual particles of various sizes. A spherical harmonic mathematical analysis can then be used to completely characterize the three-dimensional shape of each extracted aggregate. This real shape information can then be incorporated into algorithms for simulating the rheology of suspensions (fresh concrete or other materials) and into algorithms for simulating the structure of portland cement concrete.

Key Words: Aggregate, rheology, shape, spherical harmonics, suspensions, tomography, x-ray

Introduction

Crushed and naturally rounded aggregates come in all shapes and sizes. Since aggregates comprise the bulk of the volume in concrete, whether the matrix is asphalt or portland cement paste, the aggregate shape will play a crucial role in determining the properties of the composite material in which they are embedded [1,2]. Two-dimensional (2-D) information, as obtained from microscopy or other imaging systems, is often biased, especially in the case of aggregates with low sphericity, and is not sufficient to properly characterize the three-dimensional shape. True three-dimensional (3-D) information is needed.

In this paper, we show how this kind of detailed 3-D information can be acquired via x-ray computed tomography (CT). Mathematical "burning" algorithms can be applied to a multi-aggregate image to extract individual particles of various sizes. A mathematical analysis based on spherical harmonics can then be used to completely characterize the three-dimensional shape of each extracted aggregate. This real shape information can be incorporated into algorithms for simulating the rheology of suspensions (fresh concrete or other materials) and into algorithms for simulating the structure of hardened portland cement concrete and other composites.

The following sections briefly describe the process of acquiring, analyzing, and using the 3-D aggregate information in a process mixing real images and computational techniques. This research is part of a larger effort, which unites the computational and experimental materials science of building materials to develop standards and tools useful to industry and to predict material performance. This process is exemplified by the Virtual Cement and Concrete Testing Laboratory [3], which unites the experimental capabilities of leading industries with the experimental and computational expertise of the National Institute of Standards and Technology (NIST) to develop a software tool for concrete that will make possible the engineered design of new concretes in a similar spirit to how the pharmaceutical industry now designs new drugs.

X-Ray Computed Tomography

X-ray computed tomography (CT) offers a nondestructive technique for visualizing features in the interior of opaque solid objects to obtain digital information on their 3-D geometry and topology. In the simplest approach, directing planar X-rays that pass through the specimen along several sequences of paths, in several different directions, produces the set of CT images. The

intensity of X-rays is measured after it passes through the specimens. The scanning of a slice is complete after collecting the intensity measurements for a full rotation of the specimen. The specimen is then shifted vertically by a fixed amount and the entire procedure is repeated to generate additional slices. The minimum thickness of the slice, on the order of one millimeter, is set by X-ray tube and detector slit geometry. Reference [4] gives a good introduction to the general subject of CT.

The 3-D shape of the aggregate particles in a real concrete sample was captured using an X-ray CT system located at the Turner Fairbank Highway Research Center. Concrete prisms with a 75 mm x 75 mm cross sectional area were cast. The mix designs for all the prisms had a water/cement mass ratio of 0.5, with quartz sand used as the fine aggregate, and limestone used as the coarse aggregate. An industrial CT system operating at 420 keV and a 512 channel digital detector [5] was utilized to acquire images of the prisms. Horizontal slices of 0.5 mm thickness were captured every 0.4 mm and were saved in raw data format. The 20 % overlap was to ensure that all internal structures were captured in the image. The raw data were then transformed using a back projection reconstruction algorithm to generate a TIF format image. The captured image consists of 256 levels of gray intensity that correspond to different densities within the specimen. The gray scale image was then thresholded to a black and white image by recovering the known volume of aggregates contained in the sample.

Figure 1 shows a 270^3 pixel portion of the final result, cut out of the original image (this size was chosen only for convenience, as much larger samples can be handled). Aggregates (high density) in Fig. 1 appear white, while the matrix, consisting of cement paste and any unresolved fine aggregate particles, appears black. The large flat areas on the aggregates showing on the faces of the cube are from the cut through the sample, and are not real. The pixels have real dimensions of approximately 0.4 mm per pixel in all directions. The physical size of the concrete sample shown in Fig. 1 is then about 108 mm x 108 mm x 108 mm. The image shown in Fig. 1 represents preliminary work, and was taken for the purpose of developing the mathematical algorithms described in subsequent sections.

Particle Acquisition and Shape Analysis

Given that a 3-D multi-aggregate image has been obtained, one can proceed to extract individual particles. Ideally, the image should be taken of a system with a fairly low volume percent of aggregate, say 20 %, so that on the average, most particles are not near each other. The image in Fig. 1, however, was of a real concrete at a practical aggregate volume percentage (around 60 %). Because of this fact, when the 3-D image was made, many particles appeared to be in contact. This is also due partly to the fairly coarse resolution of the image, as described above, which would make many close but not touching contacts to appear as real contacts. Also, the very nature of x-ray CT causes the exterior of particles to be a little bit "fuzzy", so a large aggregate volume will result in some artificial "touches." This situation can be handled with a simple erosion and dilation algorithm [6], which breaks apart the tenuously connected aggregates, without significantly changing their size.

We next describe the "burning" algorithm that was used to identify single particles. It is quite analogous to that algorithm used in percolation studies, both in digital, pixel-based models [7-9], and in continuum model studies [10]. Imagine a 3-D cube of pixels, where each pixel is labeled either matrix (1) or particle (2). Assume for now that no particle is touching any other particle. We will also stay away from the boundaries, so that the proper boundary conditions are not a consideration. Scan through the image until a pixel is found that has label "2." Now find all nearest neighbors (back-front, left-right, up-down) of this pixel that also have label "2." Save the locations of these pixels, and then again find all neighbors of these pixels that also have the same label. Iterate this process until no more pixels of label "2" can be found. The collection of pixels found constitutes a single particle. Figure 2 illustrates this process in two dimensions.

The center of mass of this collection of pixels is computed, simply by finding the average of the (i,j,k) labels defining the pixels. Taking this point as the origin for the particle, the pixels making up the particle are then stored in terms of their (i,j,k) label relative to the center of mass of the particle.

A solid particle can be described by the function r (θ,ϕ), where r is the distance from the center of mass point to the particle surface along the direction specified by the two angles θ,ϕ from spherical polar coordinates. The unit vector along this direction is $\sin\theta \cos\phi$ **i** + $\sin\theta \sin\phi$ **j** + $\cos\theta$ **k**, where **i**, **j**, and **k** are the usual Cartesian unit vectors. The function r is numerically

determined at about 10,000 choices of the angle pairs, using the pixel collection taken from the tomograph.

The function r can be analyzed using spherical harmonics, a mathematical method often encountered in quantum mechanics [11] and in shape analysis of molecular orbitals [12,13]. For any function f(θ,ϕ), defined on the surface of a sphere ($0 < \phi < 2\pi$ and $0 < \theta < \pi$), the spherical harmonics form a complete set [14]:

$$f(\theta,\phi) = \sum_{n=0}^{\infty} \sum_{m=-n}^{n} a(n,m) Y_n^m(\theta,\phi)$$

where $Y_n^m(\theta,\phi)$ is a spherical harmonic function of order (n,m) and a(n,m) is a numerical coefficient [14]. Typically n=20 to n=30 is a high enough order to go to in the series above to capture the shape of most particles. Work is underway to determine the optimum range of n.

A simple way of seeing how well the spherical harmonic series captures the shape of a real particle is displayed in Fig. 3. This figure shows three sets of real particles, as taken from the interior of Fig. 1, in yellow, alongside the shape as derived from the spherical harmonic expansion, in purple. It is clear, even from these 2-D images, that the spherical harmonic expansion does indeed capture the shape of the real particle well. Seeing the particles in a 3-D imaging package confirms this belief. The actual size of the long dimension of the particles was about 10 mm to 20 mm.

There are two main results of this particle analysis process. First, many functions of the particle shape and size can now be analytically calculated, including volume, surface area, moment of inertia, and others. Second, these particles now have a fairly simple mathematical form, like that of a sphere or ellipsoid, so that they can be incorporated into a model like the hard core soft shell model for concrete microstructure [15,16]. This will allow real aggregate shapes to play a role in models that before used only simple shapes like spheres and ellipsoids [17]. An additional benefit will be the ability to construct databases of 3-D aggregate shapes corresponding to various aggregate sources.

Rheology Simulation

The computational modeling of complex fluids systems like suspensions presents a significant challenge, largely because it is difficult to track the boundary between a fluid and a solid phase. Recently, a new computational method called dissipative particle dynamics (DPD) has shown great promise for modeling such systems [18-20].

We have carried out extensive simulations to validate the DPD approach for modeling suspensions. For example, our rheology codes recover the Einstein prediction of the intrinsic viscosity for the case of a very dilute suspension of spheres. We have also tested our algorithms for the case of a dense suspension of monosize spheres. While there is no accepted theory for predicting the rheological properties of such suspensions, we have found good agreement with experimental data [21,22]. Figure 4 shows the reduced viscosity vs. Peclet number for different solid fractions. The Peclet number describes the competition between hydrodynamic forces due to shear and Brownian motion. For Pe > 1, hydrodynamic forces dominate, while Brownian forces dominate for Pe < 1. In most problems of interest to the aggregate industry, the Peclet number is much bigger than 1, so that hydrodynamic forces dominate. Experimental data are also included in Fig. 4 from studies of silica particles [23]. Note the good agreement over a wide range of solid fractions. The experimental and computational uncertainties are given in the caption of Fig. 4.

While our initial studies have focused on validating our DPD-based algorithms for the case of the flow of suspensions composed of uniform shaped objects (e.g. single size sphere and ellipsoids), we have begun to study the role particle size distribution plays in controlling the rheological properties of suspensions. Figure 5 shows a multi-size spherical aggregate system where the aggregates are approximately consistent with an ASTM coarse aggregate specification [24]. We are also applying the DPD code to studying the rheological properties of realistic shaped particles based on tomographic images of concrete, as in Fig. 1 above. Once the tomographic image has been processed with the burning algorithm to identify each particle, the individual digitized aggregate images can be used as templates to construct a set of rigid body inclusions that may be input into the DPD-based rheology code. Studies of such systems are currently being pursued.

Conclusion

We have shown how a combination of x-ray tomography, image analysis-type techniques, and spherical harmonic analysis can give a complete 3-D mathematical characterization of an aggregate particle. Detailed information about the particle can be obtained from this description. The derived mathematical form of the real particle also allows incorporation of the particle into various algorithms, allowing real particle shape to be used in models that before only were able to use simple shapes like spheres and ellipsoids. Databases of 3-D aggregate shape can be constructed, characterizing various aggregate sources. The rheology of a suspension of real particles can now be simulated with good accuracy, which should result in a useful computational tool for concrete.

References

1. J.F. Douglas and E.J. Garboczi, Intrinsic viscosity and polarizability of particles having a wide range of shapes, Adv. Chem. Phys. **91**, 85-153 (1995).
2. E.J. Garboczi and J.F. Douglas, Intrinsic conductivity of objects having arbitrary shape and conductivity, Phys. Rev. E **53**, 6169-6180 (1996).
3. http://vcctl.cbt.nist.gov/
4. B.P. Flannery, H.W. Deckman, W.G. Roberge, and K.L. D'Amico, Three-Dimensional X-ray Microtomography, Science **237**, 1439-1443 (1987).
5. ACTIS 600/420 Real-Time Radiography/Digital Radiography/Tomography, Report, Bio-Imaging Research, Inc. (BIR), Lincolnshire, IL, 1998.[#]
6. K.R. Castleman, *Digital Image Processing* (Prentice-Hall, Inc., Englewood Cliffs, NJ, 1979).
7. E.J. Garboczi, M.F. Thorpe, M. DeVries, and A.R. Day, Universal conductivity curve for a plane containing random holes, Phys. Rev. A **43**, 6473-6482 (1991).
8. D.P. Bentz and E.J. Garboczi, Percolation of phases in a three-dimensional cement paste microstructural model, Cem. Conc. Res. **21**, 325-344 (1991).
9. E.J. Garboczi and D.P. Bentz, The effect of statistical fluctuation, finite size error, and digital resolution on the phase percolation and transport properties of the NIST cement hydration model, submitted to Cem. Conc. Res. (2000).
10. E.J. Garboczi, K.A. Snyder, J.F. Douglas, and M.F. Thorpe, Geometrical threshold of overlapping ellipsoids, Phys. Rev. E **52**, 819-828 (1995).
11. L.I. Schiff, *Quantum Mechanics* (McGraw-Hill, New York, 1968). See Section 14.
12. N.L. Max and E.D. Getzoff, Spherical harmonic molecular surfaces, IEEE Comp. Graphics & Appl. **8**, 42-50 (1988).
13. D.W. Ritchie and G.J.L. Kemp, Fast computation, rotation, and comparison of low resolution spherical harmonic molecular surfaces, J. Comp. Chem. **20**, 383-395 (1999).
14. G. Arfken, Mathematical Methods for Physicists (Academic Press, New York, 1970). See Chapter 12.

[#] Certain commercial companies are named in order to adequately specify the experimental procedure. This in no way implies endorsement or recommendation by NIST.

15. D.N. Winslow, M.D. Cohen, D.P. Bentz, K.A. Snyder, and E.J. Garboczi, Percolation and porosity in mortars and concretes, Cem. Conc. Res. **24**, 25-37 (1994).
16. D.P. Bentz, E.J. Garboczi, and K.A. Snyder, A hard-core/soft-shell microstructural model for studying percolation and transport in three-dimensional composite media, National Institute of Standards and Technology Internal Report 6265 (1999).
17. D.P. Bentz, J.T.G. Hwang, C. Hagwood, E.J. Garboczi, K.A.Snyder, N. Buenfeld, and K.L. Scrivener, Interfacial zone percolation in concrete: Effects of interfacial thickness and aggregate shape, in *Microstructure of Cement-Based Systems/Bonding and Interfaces in Cementitious Materials*, edited by S. Diamond et al. (Materials Research Society Vol. 370, Pittsburgh, 1995), pp. 437-442.
18. P.J. Hoogerbrugge and J.M.V.A. Koelman, Simulating microscopic hydrodynamic phenomena with dissipative particle dynamics, Europhys. Lett. **19**, 155-160 (1992).
19. P. Espanol and P.B. Warren, Dissipative particle dynamics: Bridging the gap between atomistic and mesoscopic simulation, Europhys. Lett. **30**, 191-196 (1995).
20. R.D. Groot and P.B. Warren, Dissipative particle dynamics: Bridging the gap between atomistic and mesoscopic simulation, J. Chem. Phys. **107**, 4423-4435 (1997).
21. J.M.V.A. Keolman and P.J. Hoogerbrugge, Dynamic simulations of hard-sphere suspensions under steady shear, Europhys. Lett. **21**, 363-368 (1993).
22. N.S. Martys and R.D. Mountain, Velocity Verlet algorithm for dissipative-particle-dynamics-based models of suspensions, Phys. Rev. E **59**, 3733-3736 (1999).
23. Courtesy of Zhendong Cheng, EXXON.
24. Standard C33, in ASTM C09 standard book.

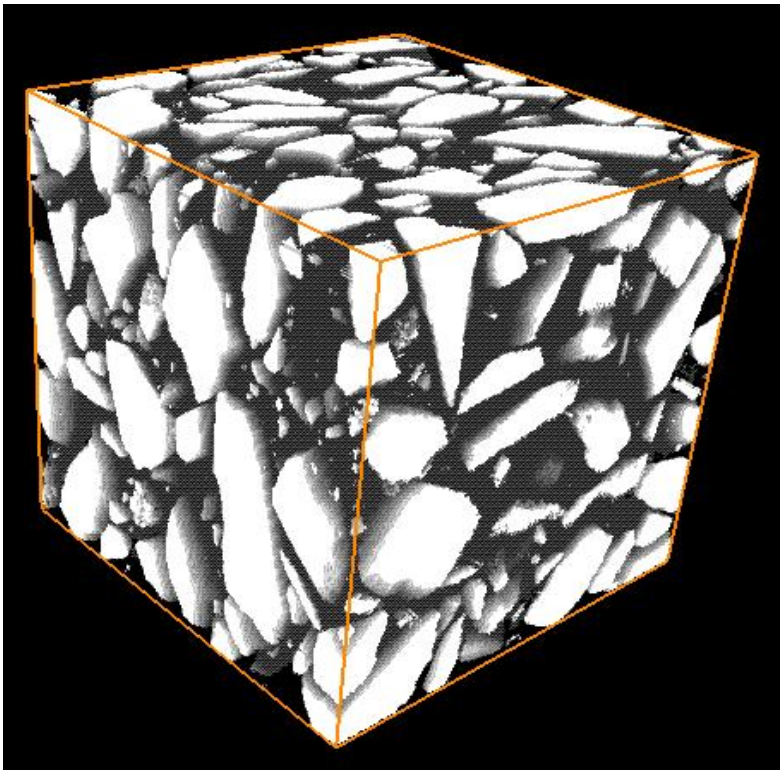

Figure 1: Reconstructed x-ray computed tomograph of a concrete specimen (270 x 270 x 270 pixels)(about 108 mm x 108 mm x 108 mm). This cube has been "cut" from a larger image, so that the flat faces of the aggregates at the surfaces are artificial.

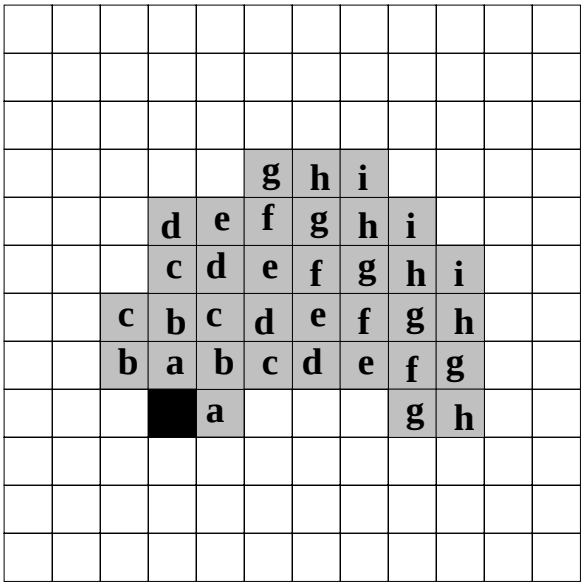

Figure 2: Showing a model particle in two dimensions (gray) embedded in a matrix (white). The black pixel shows the first particle pixel that is found by the burning algorithm. The pixels found at each iteration are labeled a-i. Nine iterations were necessary to "find" the complete particle.

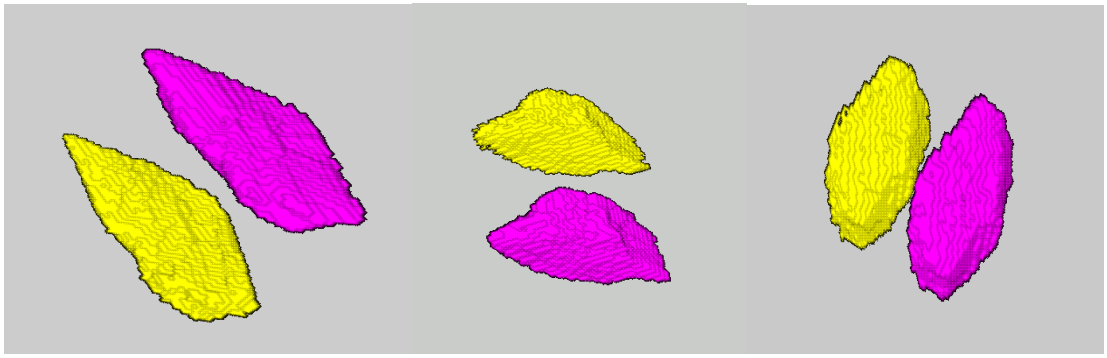

Figure 3: Three different sets of particles, comparing the real particle (yellow) as taken from the tomograph of Fig. 1 and the particle as re-created from its spherical harmonic expansion (purple). The long dimension of each particle is about 10 mm to 20 mm.

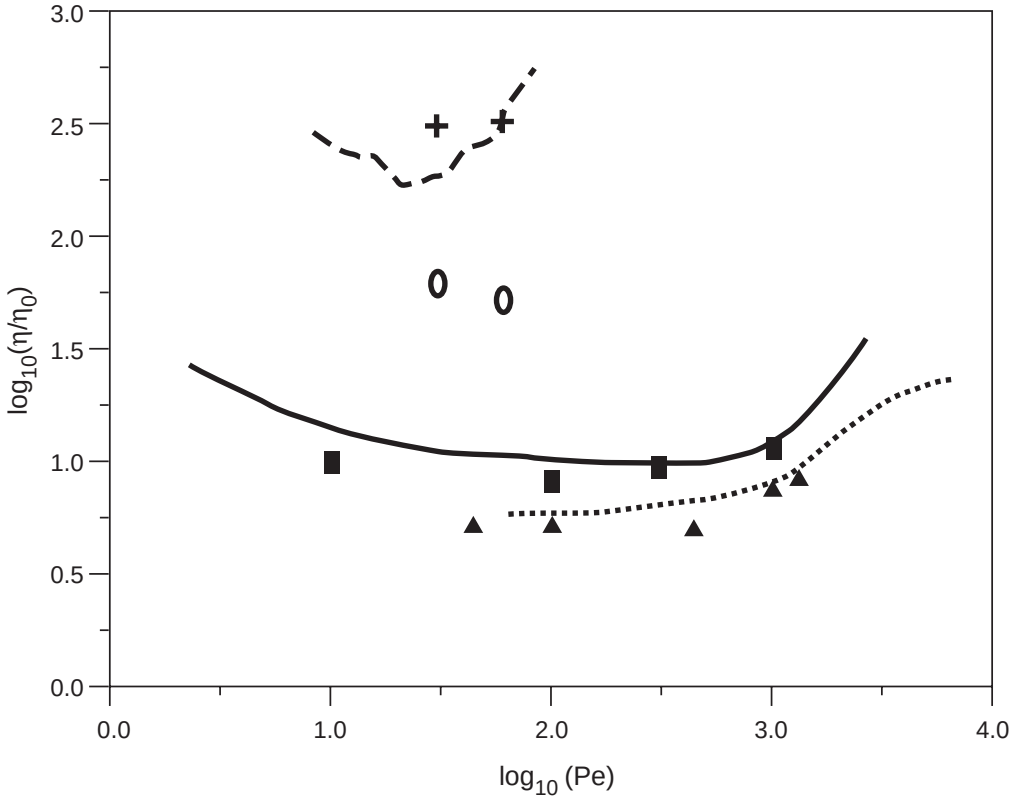

Figure 4: Log-log plot of experimental and computational viscosities vs. Peclet number. The particle volume fraction is denoted as ϕ. The lines represent experimental data from sheared suspensions of silica particles (dashed line ϕ=0.60, solid line ϕ=0.48, dotted line ϕ=0.44) and the points correspond to data from the DPD simulation (plus signs ϕ=0.60, open circles ϕ=0.50, filled squares ϕ=0.46, and filled triangles ϕ=0.40). Note that there are no experimental data to compare to the ϕ=0.50 computational data. The experimental uncertainties are approximately 10 %, and there is approximately 5 % uncertainty in the computational results (due to statistical uncertainty).

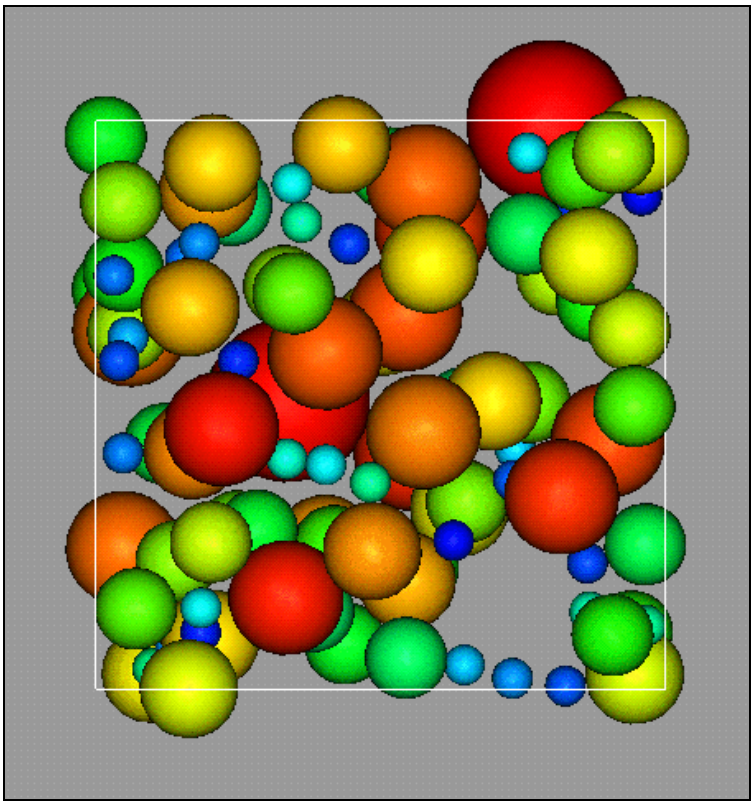

Figure 5: A multi-size spherical aggregate system where the aggregate PSD is approximately consistent with an ASTM C33 coarse aggregate specification. The picture is from the dissipative particle dynamics unit cell.

TO PAGE 1